Structure and properties of nanostructured ZrN coatings obtained by vacuum-arc evaporation using RF discharge

Anton Taran,[1] Igor Garkusha,[1] Valerij Taran,[1] Renat Muratov,[1] Vadym Starikov,[2,*] Alexey Baturin,[2] Tamara Skoblo,[3] Svetlana Romaniuk[3] and Athanasios G. Mamalis[4,*]

[1] *Institute of Plasma Physics of NSC KIPT, Kharkov, Ukraine;*
[2]*National Technical University "Kharkov Polytechnic Institute", Kharkov, Ukraine;*
[3]*National Technical University of Agriculture, Kharkov, Ukraine;*
[4]*Project Centre for Nanotechnology and Advanced Engineering, NCSR "Demokritos", Athens, Greece*

Nanostructured films of zirconium nitride have been synthesized using an ion plasma vacuum-arc deposition technique in combination with a high-frequency (RF) discharge on AISI 430 stainless steel at 150 °C. Structural examination using X-ray fluorescence (XRF), X-ray diffraction (XRD), scanning electron microscopy (SEM) with microanalysis (EDX), transmission electron microscopy (TEM), and nanoidentation was undertaken to reveal phase and chemical composition, surface morphology, microstructure and nanohardness of the coatings. The developed technology provided low-temperature film synthesis, minimized discharge breakdown decreasing formation of macroparticles (MPs) and allowed to deposit ZrN coatings with hardness variation 26.6–31.5 GPa and enhanced corrosion resistance characteristics. It was revealed that ZrN single-phase coatings of cubic modification with fine-crystalline grains of 20 nm in size were formed. The corrosion resistance of coatings has been tested in 0.9% quasiphysiological NaCl solution.

Keywords: coating, corrosion, RF-discharge, structure, vacuum-arc deposition, zirconium nitride

* Corresponding authors. E-mail addresses: vadym_starikov@ukr.net; a.mamalis@inn.demokritos.gr

doi: 10.4024/N15TA18A.ntp.14.03

1. Introduction

Zirconium nitride (ZrN) ceramic with cubic structure has high wear, fatigue and corrosion resistance and is widely used as a hard, refractory and bioinert coating in industry and medicine.[1–4] The crystal structure and mechanical properties of ZrN are similar to TiN, but the ZrN lattice parameter exceeds that of TiN (for ZrN, a = 4.58 Å and for TiN, a = 4.24 Å).[5–7] According to the Zr-N phase diagram there are stoicheiometric ZrN and nonstoicheiometric metastable Zr_2N, ZrN_2, Zr_3N_4 and Zr_4N_3 phases.[8] Hardness and elastic modulus of the ZrN coating are around 25 and 420 GPa respectively.[9–11] Wear test results indicated that ZrN is similar to titanium nitride in conventional metal cutting applications, but outperforms TiN by a factor of two when cutting titanium and aluminum alloys.[12] ZrN has also an aesthetic advantage over TiN, having a light gold colour similar to that of elemental gold.

ZrN is also considered as a biocompatible coating for various kinds of implants and coatings for surgical instruments. In accordance with ISO 10993-1 guidelines for materials that experience short-term body contact, ZrN is acceptable for external and internal medical devices that contact bone, skin tissue or blood, along with TiN, TiAlN and AlTiN. Coated implants allow the occurrence of infiltrates in the human body to be significantly reduced, avoiding the allergic and toxic reactions that otherwise may occur.[13] The bioinertness of structures made from ZrN is four times better than that of medical stainless steel. It is important to note that stainless steel does not have the required level of bioinertness due to its high nickel content.

Corrosion processes due to contact with the physiological environment should be avoided or minimized in orthopaedic implants. The body fluid environment may decrease the fatigue strength of the metal implant and enhance the extraction of iron, chromium, nickel and titanium ions, which are powerful allergens and carcinogens.[14] From this point of view TiN and ZrN PVD coatings are interesting due to their high corrosion resistance in various relevant solutions.

ZrN thin films have been synthesized by various CVD and PVD deposition methods.[15–17] It is well known that PVD technology can be used to modify the surface properties of tools without changing the underlying material properties and biomechanical functionality.

---

1 W.J. Chou, C.H. Sun and G.P. Yu, *J. Mater. Chem. Phys.* **82** (2003) 228–233.
2 A. Mitsuo, T. Mori, Y. Setswhar, S. Miyake and T. Aizawa, *Nucl. Inst. Meth. B* **206** (2003) 366–370.
3 M.M. Larijani, M. Kiani, M. Tanhayi and A. Majdabadi, *J. Cryst. Res. Technol.* **46** (2011) 351–356.
4 M. Banerjee, N.B. Srinivasan, H. Zhu et al., *J. Crystal Growth Design* **12** (2012) 5079–5089.
5 P.L. Brown, E. Curti and B. Grambow, *Chemical Thermodynamics of Zirconium*, vol. 8. Amsterdam: Elsevier (2005).
6 PDF-card No. 00-035-0753. JCPDS-International Center for Diffraction data (1998).
7 PDF-card No. 00-038-0753. JCPDS-International Center for Diffraction data (1998).
8 A. Rizzo, M.A. Signore, L. Mirenghi, and D. Dimaio, *Thin Solid Films* **515** (2006) 1486–1490.
9 L. Rogström, L.J.S. Johnson, M.P. Johansson, M. Ahlgren, L. Hultman and M. Odén, *Thin Solid Films* **519** (2010) 694–699.
10 Y. Dong, W. Zhao, Y. Li and G. Li, *J. Appl. Surf. Sci.* **252** (2000) 5057–5062.
11 M. Nose, W.A. Chiou, M. Zhou, T. Mae and M. Meshii, *J. Vac. Sci. Technol. A* **20** (2002) 823–830.
12 P.C.Johnson and H.Randhawa, *J. Surf. Coating Technol.* **33** (1987) 53–62.
13 X. Liu, P.K. Chu and C. Ding, *J. Mater Sci. Engng*, **47** (2004) 49–121.
14 D.J. Blackwood, In: *Shreir's Corrosion*, 4th edn, vol. 2, pp. 1308–1322. Elsevier (2010).
15 D.J. Kim, M.H. Lee, D.Y. Lee and J.S. Han, *J. Biomed. Mat. Res.* **53** (2000) 438–440.
16 H. Ma, J.H. Huang and H. Chen, *Surf. Coatings Technol.* **133/134** (2000) 289–294.
17 L. Pichon, A. Straboni, T. Girardeau and M. Drouet, *J. Appl. Phys.* **87** (2000) 925–930.

Plasma-based PVD coatings have favourable residual stresses, higher density and better adhesion compared to other techniques. One of the drawbacks of this method is the formation of macroparticles by the ejected molten droplets from the hot cathode spot by the higher plasma pressure within the cathode spot. The composition of these particles is completely different from the rest of the coatings, hence these particles engender a local source of variation in physical and mechanical properties.[18] The voids surrounding the macroparticles are created by the shadowing effect of the incident ion flux and such voids are expected to act as stress concentrators that facilitate crack initiation. Previous studies have shown that both flank wear and rake wear of the tool are accelerated in the presence of macroparticles. The presence of macrodefects can also result in accelerated corrosion of the underlying substrate, due to localized corrosion such as galvanic, pitting and crevice corrosion.[19]

The utilization of vacuum-arc evaporation with RF discharge allows coatings to be applied onto dielectrics and thermolabile instruments at low temperature, concomitantly decreasing the amount of macroparticles emitted from the plasma flow.

In the present paper ZrN coatings were obtained on AISI 430 stainless steel substrates using the vacuum-arc deposition technique with a high-frequency discharge régime (RF) at 150 °C. Special attention was paid to functional properties of the obtained coatings dependent on the microstructure (grain size, phase composition, nanohardness) to settle the correlation between structure–phase conditions and mechanical properties of the coatings. Deposited ZrN films have also been analysed for their corrosion properties in 0.9% NaCl quasiphysiological solution.

2. Experimental

ZrN coatings were synthesized using the vacuum-arc method with RF discharge in a Bulat-6 type device.[20–23] Bias potential was applied to the substrate from the RF generator, which produced impulses of oscillations at 5 MHz.

Chemically pure zirconium (99.999%) was used as cathode material. Nitrogen (99.999%) was used as an active gas.

Polished stainless steel samples (AISI 430) of 25 × 25 × 3 mm size were used as the substrate material (roughness $R_a \approx 0.09$ μm). The chemical composition of AISI 430 according to XRF data is presented in Table 1.

Table 1. Chemical composition (weight%) of AISI 430 stainless steel.

C	Mn	P	S	Si	Cr	Fe
0.12	1.0	0.035	0.03	1.0	17.0	81

[18] M.H. Shiao, Z.C. Chang and F.S. Shieu, *J. Electrochem. Soc.* **150** (2003) 320–324.
[19] C. Liu, A.Leyland and A.Matthews, *Corrosion Sci.* **45** (2003) 1243–1256.
[20] T.S. Skoblo, S.P. Romaniuk, A.I. Sidashenko, I.E. Garkusha, A.V. Taran et al., *J. Adv. Microsc. Res.* **13** (2018) 333–338.
[21] A.V. Taran, I.E. Garkusha, V.S. Taran et al., *J. Adv. Microsc. Res.* **13** (2018) 313–319.
[22] V. Tereshin, V. Taran et al., *Vacuum* **73** (2003) 555–559.
[23] V. Gasilin, O. Svets, V. Taran et al., *J. Appl. Plasma Science* **13** (2005) 87–93.

Before deposition, the substrates were precleaned in an ultrasonic bath for 10 min. Surface cleaning (substrate degreasing and removing impurities) in the RF discharge was carried out in an argon plasma for 15 min (U_{bias} = 1000 V, P(A) = 0.6 Pa). A Zr buffer layer of 20 nm thickness was deposited before the nitride coating to improve coating adhesion, using I_{arc} = 110 A, $U^{(RF)}_{bias}$ = –200 V, base pressure $P = 5 \times 10^{-4}$ Pa and deposition time = 25 min.

The surface topography was studied using a JEOL JSM-6390LV scanning electron microscope (SEM) with an accelerating voltage of 20 kV; the chemical composition was examined using EDX analysis.

The microstructure and phase composition were investigated by transmission electron microscopy (TEM) using an EMV-100L instrument with an accelerating voltage of 100 kV. The ZrN coatings of 70 nm thickness were synthesized on chipped (001) KCl crystals for the TEM using the same deposition parameters.

A SPRUT-K energy-dispersive spectrometer (AO Ukrrentgen, Ukraine) was used for X-ray fluorescence (XRF) analysis equipped with a Si (Li) X-100 detector (Amptek, USA) in the arrangement with a Si and KCl secondary target. A BS-22 X-ray tube with a shoot-through type Ag anode was used (U = 35 kV, I = 250 A and exposure time = 300 s). Film thickness was determined by XRF examination; the average film thickness was 1.67 μm.

X-ray diffraction (XRD) analysis were undertaken using a DRON-3M device, under Cu–Kα radiation, made monochromatic by highly oriented (002) pyrolytic graphite (HOPG) in the diffracted beam. The XRD line scans were done in the θ–2θ scanning mode, where the incident angle θ and the diffracted angle 2θ are scanned simultaneously.

The nanohardness was measured with a G200 Nanoindenter (USA). The loading and unloading rates of the nanoindentation were 10 mN/min. Samples were tested to a depth of 500 nm. The distance between nanohardness indentations was 15 μm and for each sample 7 indentations were made.

The electrochemical activity (corrosion properties) of the ZrN coatings was determined by the values of their electrode potentials (reference electrode: AgCl). The measurements were carried out in an electrochemical cell filled with 0.9% w/w aqueous NaCl (quasiphysiological solution).

3. Results and discussion

3.1 Structure, chemical and phase composition

A typical XRD pattern of a ZrN coating obtained in the RF régime is presented in Fig. 1. The ZrN phase diagram is shown in Fig. 2. All angles of diffraction peaks with (111), (222) and (220) main reflexions were indexed as the ZrN phase with a crystal structure of the B1 NaCl cubic lattice type (according to JCPDS 35-0753, lattice constant a = 0.4577 nm). The high intensity of the ZrN (111) Bragg peak indicates that the ZrN grains grow with the [111] preferred orientation, perpendicular to the growth plane.

For transition metal nitrides with a NaCl-type lattice, which have local octahedral atomic coördination, periodic alternation of atomic layers fully occupied with only metal or non-metal (nitrogen) atoms occurs along the [111] direction. Such arrangement of the layers corresponds to the lowest surface free energy of the system and is the most frequently encountered case, especially with low stresses developing in the condensate and at the initial stages of film growth. The [111] texture was also ascertained for various other films

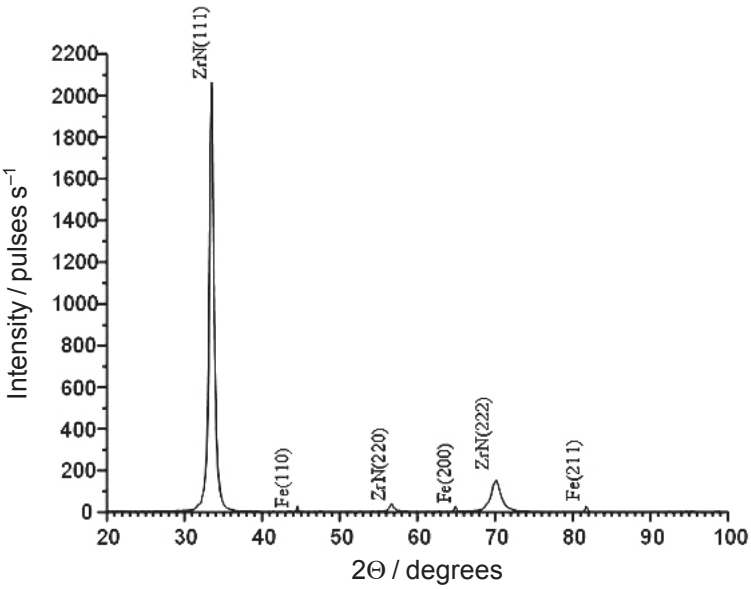

Figure 1. XRD spectra of ZrN coating.

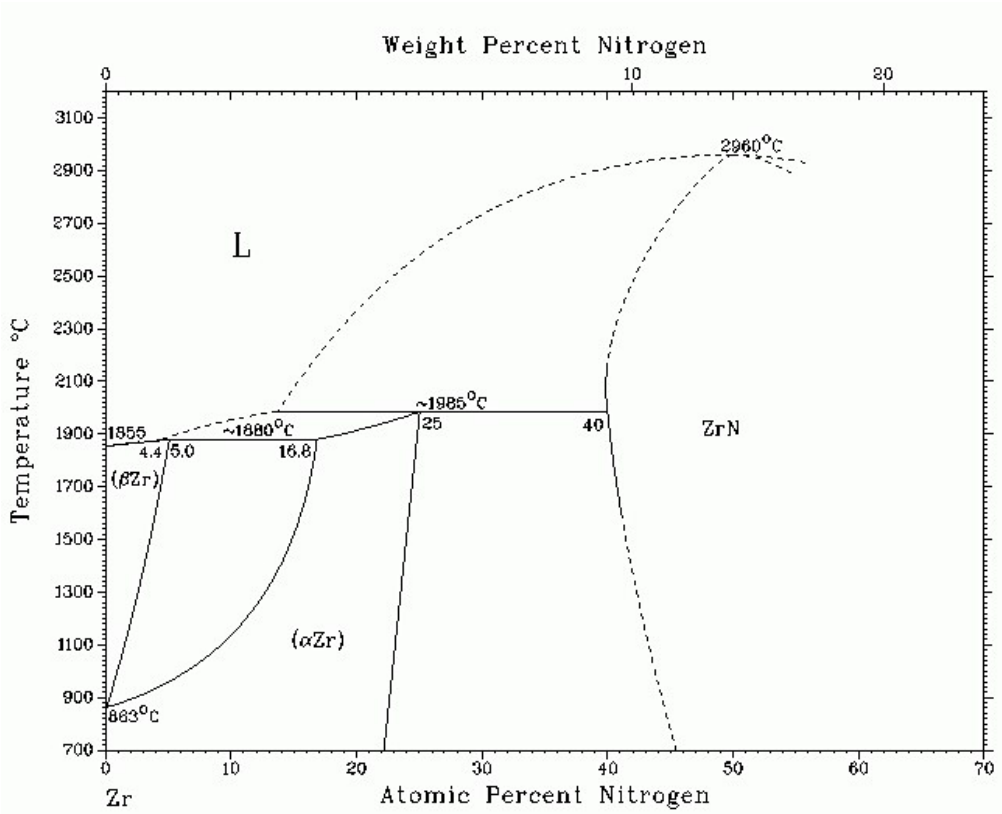

Figure 2. ZrN phase diagram.

(TiN, CrN, TiAlN, TiCN) deposited by the cathodic arc technique.[24, 25] The presence of highly ionized plasma also favours film growth in the most densely packed direction.[26, 27]

The XRD peak width indicates fine-crystalline structure with an average grain size of 15–20 nm. The high-frequency technique leads to a smaller average crystallite size in comparison with the standard PVD mode due to a higher density of crystal nuclei during formation. The microdeformability of crystallites was also smaller using the RF method.

The XRD data correlates well with the TEM results, shown in Fig. 3.

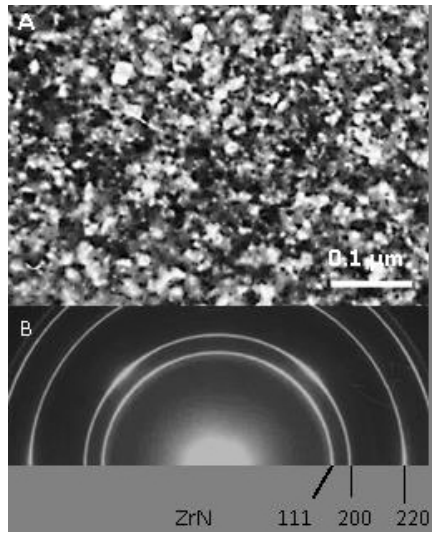

Figure 3. A. TEM image; and B, electron diffraction pattern of ZrN on (001) KCl.

All electron-diffraction lines were indexed as the ZrN phase with *bcc* lattice having stoichiometric composition. No additional phases have been revealed. The obtained results are summarized in Table 2. The average grain size was 0.02 μm.

Table 2. Interplanar spacings of the ZrN coating on (001) KCl.

Reference data [6]	Experiment (this work)		
d / Å	*d* / Å	*I* (%)	(hkl)
2.64	2.63	100	(111)
2.29	2.27	74	(200)
1.61	1.59	36	(220)
1.38	1.36	24	(311)
1.32	1.32	9	(222)
1.14	1.15	2	(400)

[24] R.L. Boxman and N.A. Travitzky, *Surf. Coatings Technol.* **114** (2000) 133–134.
[25] A. Bendavid, P.J. Martin, T.J. Kinder and E.W. Preston, *Surf. Coatings Technol.* **163/164** (2003) 347–352.
[26] D.C. Kothari and A.N. Kale, *Surf. Coatings Technol.* **174** (2002) 158–159.
[27] M. Balaceanu et al., *Surf. Coatings Technol.* **202** (2008) 3981–3987.

The optical microscopy images of the initial surface and the deposited ZrN coating are presented in Fig. 4, and the surface morphology and chemical composition heterogeneity from the scanning electron microscopy with EDX are shown in Figs 5 and 6. The surface is rather smooth, having a small number of macrodefects identified as drops falling from the cathode material (Fig. 6A–C). The size of the macroparticles does not exceed 4 μm. The integral chemical composition is given in Fig. 5B. The presence of a small quantity of oxygen and carbon is due to residual gas incorporated in the chamber walls and contamination during sample handling in the open atmosphere before the composition analysis. Using thermionic emission, it was monitored. The homogeneous surface distribution of selected elements is shown in Fig. 6. EDX microanalysis results taken from four local areas are presented in Table 3.

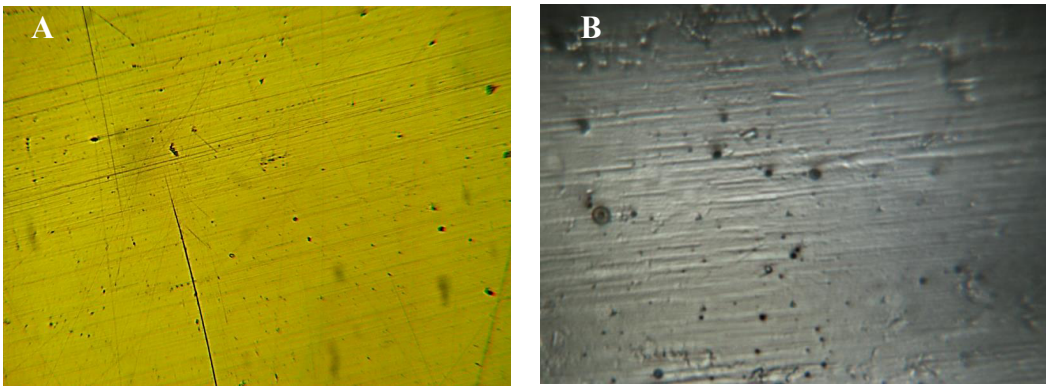

Figure 4. Light optical microscopy images of: A, the initial surface at 160×; and B, the ZrN coating at 300× magnifications.

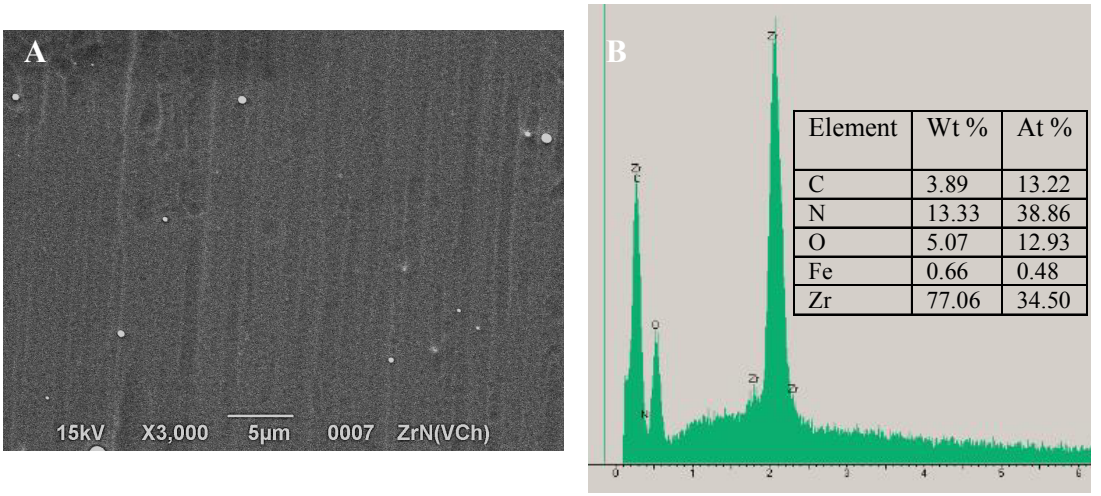

Element	Wt %	At %
C	3.89	13.22
N	13.33	38.86
O	5.07	12.93
Fe	0.66	0.48
Zr	77.06	34.50

Figure 5. A, Surface morphology and B, chemical composition of a typical ZrN coating.

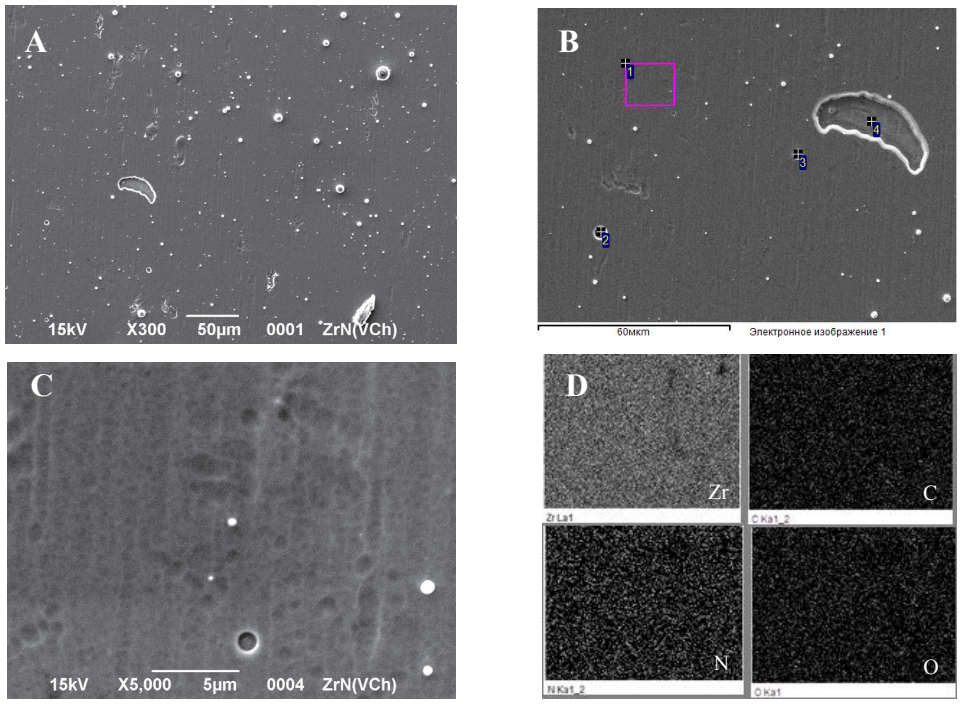

Figure 6. A–C, SEM images and D, distribution of Zr, N, C, O on the surface showing homogeneity.

Table 3. Chemical composition (weight%) from local selected areas (see Fig. 6D)

Spectrum	C	N	O	Na	Si	Cr	Fe	Zr
1	3.13	12.52	4.87				0.79	78.68
2	0.88	5.22	1.13				2.07	90.71
3	11.99	21.58	6.39				0.61	59.42
4	17.70		5.68	0.29	0.25	11.22	58.39	6.47

3.2 Mechanical properties

The microhardness of the coating strongly depends on structural parameters such as crystallographic orientation, microstress, and crystallite size. One of the main characteristics of the material is the ratio of its hardness to the elastic modulus *H/E*, called the plasticity index. The ratio H^3/E^{*2} (where $E^* = E/(1 - \mu^2)$ is the effective elastic modulus, where μ is Poisson's ratio) is a qualitative comparative characteristic of the plastic deformation resistance. To increase the plastic deformation resistance one must strive for the lowest possible elastic modulus at high hardness which, in particular, occurs at grain sizes of less than 10 nm. In general, the low modulus is good, because it allows load to be distributed over a wide area.

The effective elastic modulus E^*, the shear modulus *G*, yield stress point σ_T and coefficient of resistance to plastic deformation H^3/E^{*2} were determined using model equations. The shear

modulus and yield stress are defined as:

$$G = E / 2 \times (1 + \mu) \quad (1)$$

$$\sigma_T = H / 3 \quad (2)$$

The nanoindentation diagrams for the initial surface and with the ZrN coating are presented in Fig. 7. *H* and *E* values for 7 diamond pyramidal tips are summarized in Table 4.

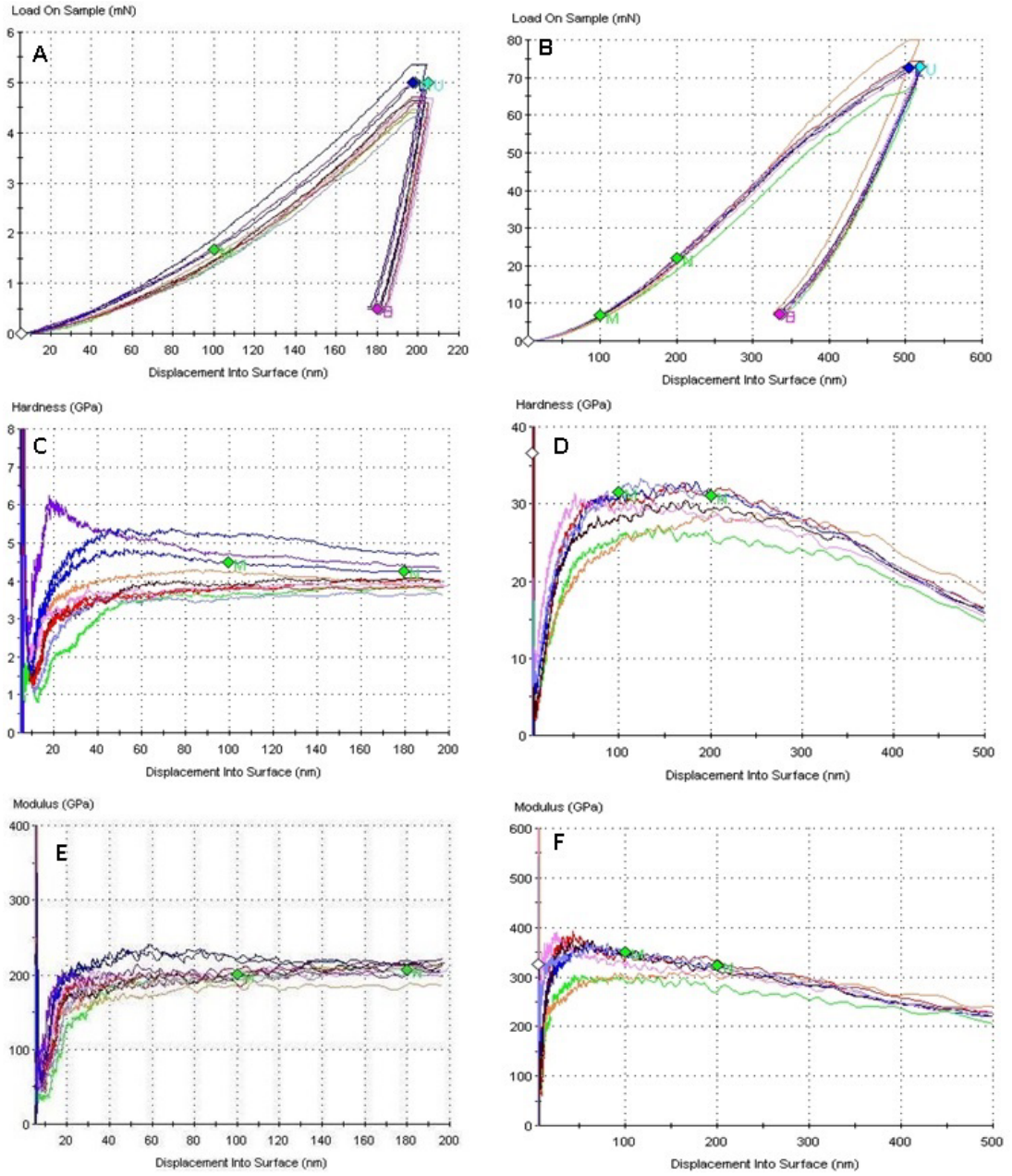

Figure 7. Nanoindentation diagrams for the initial surface (A, C, E) and the ZrN coating (B, D, F).

Table 4. Mechanical properties of AISI 430 and the ZrN coating.

	AISI 430			ZrN coating		
	E / GPa	*H* / GPa	*H/E*	*E* / GPa	*H* / GPa	*H/E*
1	204.496	3.727	0.018	336.309	31.071	0.092
2	184.049	4.084	0.021	333.475	31.576	0.094
3	203.588	3.872	0.019	288.604	26.110	0.090
4	205.773	3.990	0.019	302.027	26.635	0.088
5	198.272	3.610	0.018	316.364	29.188	0.092
6	202.134	4.559	0.022	331.657	29.140	0.087
7	209.751	3.800	0.018	337.236	32.047	0.095
Average value	201.151	4.092	0.020	320.810	29.395	0.091

The G, σ_T and H^3/E^{*2} parameters were computed only for the average H and E values (Table 4) and are presented in Table 5. According to the nanohardness tests, the ZrN coating has greatly superior elastic properties compared with the initial stainless steel. As seen from Table 4, increase of the H/E ratio implies decreased plasticity of the material and increased relative hardness. The high hardness of the coatings can be associated with an improvement of homogeneity of ZrN coatings on the one hand and on the other the hardness growth can be related to grain refinement (according to the Hall–Petch rule) by ion bombardment upon application of high-voltage RF pulses to the substrate during the deposition process.

Table 5. G, σ_T and H^3/E^{*2} parameters of AISI 430 and ZrN coating based on H and E average values (taken from Table 4).

Sample	*E* / GPa	*H* / GPa	*G* / GPa	σ_T / MPa	H^3/E^{*2}
AISI 430	201.151	4.092	62	133	0.0014
ZrN coating	320.810	29.395	121	966	0.05

3.3 Corrosion resistance

Because of the medical applications of nitride coatings, the electrode potentials of the substrate AISI 430 in the initial state and after deposition of the ZrN film were measured in 0.9% NaCl (quasiphysiological) solution (Fig. 8). Wax was used to isolate those parts of the substrate not coated with ZrN film.

The test shows that application of the nitride coating leads to substantial displacement of the electrode potential of the AISI 430 substrate to a positive range of values; that is, like the deposition of titanium dioxide. This indicates an increase of substrate resistance against electrochemical corrosion. Thus, nitride coatings can be effectively used on the surface of endoösseous implants and, taking into account their good mechanical characteristics, as coatings for surgical instruments.

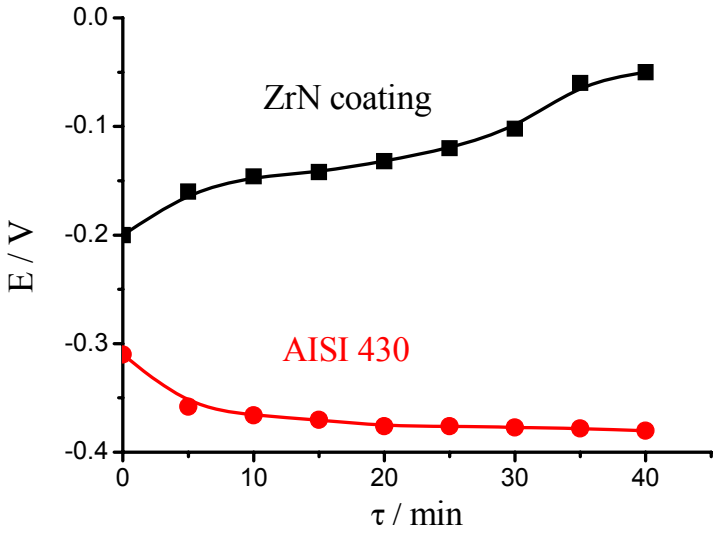

Figure 8. Electrode potentials of AISI 430 and the ZrN coating.

4. Summary and conclusions

1. Zirconium nitride coatings have been synthesized using the ion-plasma vacuum-arc deposition technique in combination with high-frequency (RF) discharge on AISI 430 stainless steel at 150 °C;
2. The proposed low-temperature deposition technology minimizes the formation of macroparticles;
3. Nanostructured single-phase ZrN coatings of the cubic modification with fine-crystalline grains of 20 nm size were formed;
4. The average values of elastic modulus and nanohardness of ZrN were 320.810 GPa and 29.395 GPa respectively;
5. The deposition of the ZrN coating leads to passivation of the metal substrate surface, which is manifested by displacement of the electrode potential to a positive range of values.